Research Square

Preprints are preliminary reports that have not undergone peer review.
They should not be considered conclusive, used to inform clinical practice,
or referenced by the media as validated information.

Direct synthesis of dimethyl carbonate from carbon dioxide and methanol over bimetallic Ce/Zr-MOF-808

Chuanfeng Li
Wuhan Polytechnic University
Yijie Zhou
Wuhan Polytechnic University
Wenyang Wang
Wuhan Polytechnic University
Guozhi Fan
fgzcch@whpu.edu.cn

Wuhan Polytechnic University

Research Article

Keywords: Carbon dioxide, Methanol, Dimethyl carbonate, Ce/Zr-MOF-808 catalyst

Posted Date: November 19th, 2026

DOI: https://doi.org/10.21203/rs.3.rs-11539953/v1

License: This work is licensed under a Creative Commons Attribution 4.0 International License.
Read Full License

Additional Declarations: No competing interests reported.

Abstract

An efficient bimetallic metal-organic framework (MOF) catalyst for the direct synthesis of DMC from from carbon dioxide (CO_2) and methanol (CH_3OH). Using zirconium chloride octahydrate, cerium nitrate hexahydrate, and 1,3,5-benzenetricarboxylic as precursors, MOF-808 with cerium-zirconium bimetallic centers (Ce/Zr-MOF-808) was readily synthesized via a one-pot hydrothermal method. Detailed characterization of Ce/Zr-MOF-808 revealed it retained the octahedral structure of MOF-808, featuring Lewis acid/base sites and the coexistence of Ce^{3+}/Ce^{4+}. Ce doping enhanced the catalytic activity of Ce/Zr-MOF-808, which exhibited promising activity and excellent stability for the conversion of CO_2 into DMC. The selectivity for DMC reached 94.24%, with 5.56% conversion of CH_3OH and 5.24% yield of DMC. After four cycles, the yield of DMC slightly decreased from 5.24% to 4.13%, retaining 78.8% of the initial activity. The reasons for the decline in the catalytic performance were revealed, it was primarily caused by the deposition of carbon-containing compounds on the catalyst surface during the reaction process. Based on investigation on the roles of acid-base sites of Ce/Zr-MOF-808 and *in situ* infrared, A potential reaction mechanism for the direct synthesis of DMC from CO_2 and CH_3OH over Ce/Zr-MOF-808 was proposed in which both Lewis acid and base active sites play crucial roles.

Highlights

λ Ce-doped Zr-MOF-808 was developed for the direct synthesis of DMC from CO and CHOH.

λ Ce doping enhanced the catalytic performance of Ce/Zr-MOF-808.

λ Ce/Zr-MOF-808 exhibited superior activity compared to similar MOF materials.

λ The synergistic effect between Lewis acid-base sites boosted DMC yield to 5.24%.

λ Catalyst showed excellent stability, retaining 78.8% initial activity after four cycles.

1 Introduction

The emission of carbon dioxide (CO_2) continues to rise [1], exerting adverse effects on global temperature changes, ecosystem, climate and biodiversity [2]. Factually, CO_2 serves as a vital source of organic carbon, offering advantages such as abundant resources, availability, recyclability and low cost [3]. Consequently, developing technologies for efficient CO_2 utilization has garnered significant attention. Converting CO_2 into high-value chemicals like methanol (CH_3OH), dimethyl ether (DME) and dimethyl carbonate (DMC) represents one pathway toward its effective utilization [4]. DMC, as a crucial chemical intermediate, contains carbonyl, methyl and methoxy groups. Through carbonylation, methylation, methyl esterification, and transesterification reactions, it can be further converted into other high-value-added chemicals [5]. Generally, DMC is synthesized via phosgene ($COCl_2$), oxidative carbonylation, transesterification and direct synthesis [6].

Although the large-scale industrial production of DMC was initially achieved via the phosgene method, phosgene is a colorless, highly corrosive and toxic gas that causes environmental pollution [7], thereby limiting its application. In oxidation-carbonylation reactions, mixtures of CO and O_2 are highly explosive, and CO itself is both flammable and toxic [8]. The transesterification method has the advantages of environmental friendliness and high product selectivity. However, the raw material cost is high, and the reaction procedures are numerous. Moreover, it is limited by thermodynamic equilibrium with low substrate conversion. Recently, the direct synthesis of DMC from CO_2 and CH_3OH has been regarded as a highly promising approach due to its environmental friendliness, safety and atom economy advantages [9, 10]. However, constrained by thermodynamic conditions and the chemical inertness of CO_2, both CH_3OH conversion and DMC yield remain at low levels [11]. Additionally, water generated during the reaction can also cause rapid catalyst deactivation. Consequently, researches on the direct synthesis of DMC primarily focused on developing highly active catalysts to reduce activation energy and efficient dehydrant to remove moisture. This facilitates the progression of the reaction toward the formation of the target product [12].

Metal oxides are widely used as catalysts for the direct synthesis of DMC from CO_2 and CH_3OH, with ZrO_2 and CeO_2 being the most common [2, 9, 11, 13]. The mechanism for the direct synthesis of DMC from CO_2 and CH_3OH over ZrO_2 was investigated by *in situ* ftourier transform infrared spectroscopy (*in situ* FTIR) [14, 15]. Research indicates that acid-base sites on the catalyst surface played decisive roles. However, ZrO_2 exhibited low activity, the yield of DMC was only 0.45% [16], and it slightly increased to 0.6% when CeO_2 nanorod was employed as a catalyst [17]. To modulate the acid-base properties, electron-rich lattice oxygen species were introduced into CeO_2 by constructing a large number of point defects and crystal-terminated phases. Catalytic activity was significantly enhanced, producing a DMC yield of 1.19% [9]. However, due to the low specific surface area and insufficient exposure of active sites in metal oxide catalysts, the DMC yield remains relatively low [18].

Metal-organic frameworks (MOFs), particularly UiO-66 and MOF-808 [11], have found extensive applications in the field of catalysis due to their tunable pore structure characteristics, high specific surface area and porosity [19–21]. Due to high specific surface area and acidic/basic active sites, UiO-66 and MOF-808, have been employed to catalyze the conversion of CO_2 into DMC. Although UiO-66 exhibits superior specific surface area and acidic/basic active sites compared to MOF-808, its catalytic activity remains relatively low. In the presence of UiO-66 and MOF-808, the DMC yields were 0.08% and 0.12%, respectively. This is attributed to larger micropore size of MOF-808, a feature that promotes substrate activation [11]. Moreover, a series of Ce-doped UiO-66 (Ce-UiO-66) catalysts were prepared by adjusting the composition of Lewis acid-base sites on the material surface. Ce doping has a negligible effect on the specific surface area of catalyst but significantly increases the number of active sites (Lewis acid and basic sites, and terminal hydroxyl). Following Ce doping, the DMC yield correspondingly increased from 0.120% to 0.295% [13].

Despite significant attention being devoted to the development of high-performance catalysts for the direct synthesis of DMC, thermodynamic limitations and the generation of water during the reaction have kept DMC yields at low levels, severely hindering the reaction process [11]. In the presence of a dehydrating agent, water molecules can be captured or consumed, shifting the reaction equilibrium toward the formation of the target product. Correspondingly, the yield of DMC was improved. Molecular sieves (MSs), trimethylene mesylate (TMM) and 2-cyanopyridine (2-CP) are common dehydrants, with 2-CP removing water via an in situ hydration reaction and being regenerated through a simple dehydration reaction [2, 11, 22]. For instance, rod-CeO_2 and 2-CP were used as the catalyst and dehydrant for the direct synthesis of DMC, respectively. The yield of DMC was enhanced from 0.08% to 0.51%, increasing about 6.5 times [23]. Moreover, 2-CP was also used for the synthesis of DMC over Ce-UiO-66, and the yield of DMC was enhanced from 0.13% to 1.22%, increasing by about 9.4 times [13]. Based on the above findings, Ce-doped MOF-808 (Ce/Zr-MOF-808) catalyst using 2-CP as the dehydrating agent is anticipated to be a efficient catalytic system for the direct synthesis of DMC from CO_2 and CH_3OH.

Herein, Ce/Zr-MOF-808 materials featuring cerium-zirconium bimetallic active centers was prepared by a one-pot hydrothermal method and characterized in detail. The catalytic performance of Ce/Zr-MOF-808 was further evaluated for the direct synthesis of DMC from CO_2 and CH_3OH by varying the regulator, ligand dosage, the molar ratio of Ce to Zr, catalyst dosage, dehydrant type and its dosage, and reaction conditions. Ce/Zr-MOF-808 exhibited excellent activity and recyclability for the conversion of CO_2 into DMC, and the catalytic performance was improved due to Ce doping. The selectivity for DMC reached 94.24%, with 5.56% conversion of CH_3OH and 5.24% yield of DMC. The yield of DMC was higher than those obtained in the presence of the similar MOF materials. After four cycles, the yield of DMC slightly decreased from 5.24% to 4.13%, and the reasons for the decline in catalytic performance was revealed. Additionally, the cyclic catalytic performance of Ce/Zr-MOF-808 was investigated, and a possible reaction mechanism was proposed based on *in situ* FTIR.

2 Experimental

2.1 Materials

Zirconium chloride octahydrate ($ZrOCl_2{\cdot}8H_2O$), cerium nitrate hexahydrate ($Ce(NO_3)_3{\cdot}6H_2O$), 1,3,5-benzenetricarboxylic (BTC), CeO_2, TMM and 2-CP were purchased from Aldrich Chemical Reagents Co. ltd. (Shanghai, China). CH_3OH, *N, N*-dimethylformamide (DMF), formic acid (FA), acetic acid (AA), benzoic acid (BA), 3A molecular sieve (3A MS), 4A molecular sieve (4A MS), 5A molecular sieve (5A MS), pyridine (Py) and DMC were purchased from Sinopharm Chemical Reagent Co. ltd. (Peking, China). CO_2 was purchased from Wuhan Minghui Gas Technology Co. ltd. (Wuhan, China). The preparation methods for UiO-66 and MOF-808 were carried out according to published literature [13, 18].

2.2 Preparation of Ce/Zr-MOF-808

In a 100 mL hydrothermal reaction vessel, 0.774 g (2.4 mmol) of $ZrOCl_2 \cdot 8H_2O$, 0.347 g (0.8 mmol) of $Ce(NO_3)_3 \cdot 6H_2O$ and 0.17 g (0.8 mmol) of BTC were added into 40 mL mixture of FA and DMF (1:1, *v*:*v*). The mixture was heated to 130 ℃, followed by stirring for 4 h before cooling to room temperature. Subsequently, the solid was collected by centrifugation, and washed three times with DMF and CH_3OH, respectively, before drying at 80 ℃ for 12 h to afford Ce/Zr-MOF-808 [24].

2.3 Synthesis of DMC over Ce/Zr-MOF-808

Typically, 0.25 g of Ce/Zr-MOF-808, 8 mL (200 mmol) of CH_3OH and 4.8 mL (50 mmol) of 2-CP were added into a 50 mL autoclave, and the air inside the autoclave was replaced by 1 MPa CO_2 for three times. The mixture was heated to 140 ℃, then pressurized to 10 MPa with CO_2. After magnetic stirring for 16 h, the reaction mixture was cooled to room temperature and depressurized slowly. The mixture was then centrifuged, and the supernatant was collected. The liquid was quantitatively analyzed by gas chromatography (GC) to determine CH_3OH conversion, DMC yield, and selectivity, as detailed in Eqs. S1 – S3.

2.4 Cyclic performance of Ce/Zr-MOF-808

After the catalytic reaction, the reaction mixture was centrifuged to separate the solid, which was collected and washed three times with DMF and CH_3OH, respectively. The solids were then dried at 80 ℃ for 12 h to obtain the recovered Ce/Zr-MOF-808. Without requiring further treatment, the recovered catalyst can be directly used in subsequent reactions.

2.5 Measurements

FTIR was performed on a Thermo Nicolet 330 Fourier transform infrared spectrometer within the measurement range of 4000 to 400 cm^{-1}. The samples were ground with dried KBr powder and compressed into a disc prior to analysis. X-ray diffraction spectroscopy (XRD) was performed on a Bruker D8 Advance X diffractometer with Cu Kα radiation and λ of 0.15406 nm at a scanning rate of 5°/min in the range of 0° to 80°. The tube voltage and tube current were 40 kV and 40 mA, respectively. N_2 adsorption-desorption testing was conducted using a Micromeritics ASAP 2020 Plus automatic static chemisorption apparatus at 77 K and the samples were degassed at 150 ℃ for 12 h prior to analysis. Thermogravimetric analysis (TGA) was performed on a Netzsch STA 449F5 Perkin-Elmer TG-DSC7 spectrometer at a heating rate of 10 ℃/min in the range of room temperature to 800 ℃ under N_2 atmosphere. Sample morphology was analyzed by Zeiss Gemini 300 scanning electron microscopy (SEM) with an acceleration voltage of 20 kV, a current of 80 μA, and a thermal field emission electron source. X-ray photoelectron spectroscopy (XPS) was conducted on a Thermo Scientific K-Alpha spectrometer. The energy and energy resolution are 100 eV and 50 eV, respectively. The C1s peak was used to calibrate the electron binding energy of the sample surface. Energy-dispersive X-ray spectroscopy (EDS) was performed on a Bruker Super-Xflash spectrometer. Temperature-programmed desorption (TPD) including CO_2-TPD and NH_3-TPD curves were measured on an AutoChem II 2920 chemisorption analyzer equipped with a thermal conductivity detector (TCD) using He as the carrier gas

in the range of room temperature to 800 ℃. Inductively coupled plasma optical emission spectrometry (ICP-OES) was conducted on an Agilent 5110 inductively coupled plasma optical emission spectrometer to determine the contents of Zr and Ce. The liquid products were quantitatively analyzed by GC 2030 gas chromatograph equipped with a flame ionization detector (FID) and a PEG-20M capillary column (30 m × 0.32 mm × 0.50 μm). *In situ* FTIR spectroscopy was performed on a Thermo Scientific Nicolet IS50 infrared spectrometer with a MCT/A detector and resolution of 32 cm^{-1} for recording the spectra in the range of 4000 to 650 cm^{-1}. The samples were sealed into an *in situ* reaction cell with ZnSe windows, and the catalyst was degassed at 180 ℃ before cooling to 140 ℃ for adsorption.

3 Results and discussion

3.1 Characterization

3.1.1 Structure characterization of Ce/Zr-MOF-808

Figure 1a shows the FTIR spectra of Ce/Zr-MOF-808 and its recovered sample after four cycles. In the FTIR spectrum of Ce/Zr-MOF-808, the bands at 1605 and 1445 cm^{-1} were attributed to C = C vibrations in the benzene ring, and 1380 cm^{-1} belonged to the symmetric vibrations of the C = O bond in the –COO groups [24–26]. Additionally, the bands at 760 and 717 cm^{-1} corresponded to the stretching vibrations of C – H and Zr – O bonds [18, 27, 28], respectively. After Ce doping, the characteristic bands of MOF-808 only exhibited slight shifts, indicating that Ce/Zr-MOF-808 retained the structure of MOF-808 [24]. Nevertheless, several new bands appeared in the FTIR spectrum of Ce/Zr-MOF-808. The band at 660 cm^{-1} belonged to the stretching vibration of Ce–O [26, 29], suggesting the coordination of – COO with Ce^{3+} [30] Since partial Ce^{3+} underwent electron loss during the preparation of Ce/Zr-MOF-808 [24], which can be captured by atmospheric oxygen atoms to form CeO_2. Correspondingly, a novel weak band attributed to the stretching vibration of Ce – O–Ce was observed at 555 cm^{-1} [31], indicating the formation of trace amounts of CeO_2. According to the FTIR results, Ce/Zr-MOF-808 with Zr-Ce bimetallic centers was successfully prepared.

Figure 1a also shows that the FTIR spectrum of the recovered Ce/Zr-MOF-808 was similar to that of fresh sample, but it exhibited a new band at 2920 cm^{-1} and weakened intensities at 660 and 555 cm^{-1}. The former was ascribed to the stretching vibration of C – H bonds in carbon-containing compounds deposited on the catalyst surface [28, 32], while the latter suggested the loss of Ce during the reaction. In addition, the band intensity at 555 cm^{-1}, corresponding to the Ce – O–Ce bond, significantly decreased, suggesting that CeO_2 was more susceptible to leaching [33]. This can be attributed to the fact that Ce^{4+} was not involved in coordination, which may primarily exist on the catalyst surface. The detachment of CeO_2 may adversely affect the cyclic catalytic performance of Ce/Zr-MOF-808, as this substance exhibits catalytic activity for converting CO_2 to DMC [11].

Figure 1b shows the XRD patterns of Ce/Zr-MOF-808 and its recovered sample after four cycles. The characteristic diffraction peaks of Ce/Zr-MOF-808 at 4.3°, 8.3°, 8.6° and 10° were attributed to (111), (311), (222) and (400) reflections, respectively. These results indicated that Ce^{3+} was incorporated into the structural unit of MOF-808 without forming a new structure [24]. However, new weak peaks at 23.7°, 29.0°, 33.6°, 48.1° and 57.0° appeared in the XRD pattern of Ce/Zr-MOF-808. The peak at 23.7° likely originated from crystal defects within the material [34], while the peaks at 29.0°, 33.6°, 48.1° and 57.0° were attributed to (111), (200), (220) and (211) reflections of the face-centered cubic fluorite structure of CeO_2 [35], further confirming the successful preparation of Ce/Zr-MOF-808 and the formation of a trace amount of CeO_2.

As shown in Fig. 1b, all characteristic diffraction peaks of MOF-808 remain presented in the XRD pattern of the recycled Ce/Zr-MOF-808, indicating that the catalyst structure is well preserved after the reaction. However, peak intensities at 4.3°, 8.3°, 8.6° and 10° were enhanced. This enhancement resulted from the promotion of nucleation within the material under elevated reaction temperatures and extended reaction times, thereby increasing the crystallinity of MOF-808 [36, 37]. This may affect the cyclic catalytic performance of the catalyst. The XRD pattern of the recovered Ce/Zr-MOF-808 also showed a decrease in the intensity of characteristic diffraction peaks attributed to CeO_2. These results indicate that CeO_2 loss occurred during the reaction process, consistent with the FTIR results shown in Fig. 1a.

N_2 adsorption-desorption isotherms and pore size distributions of Ce/Zr-MOF-808 and its recovered sample after four cycles are shown in Figs. 1c and 1d. In the low relative pressure range of 0.0 – 0.1, the adsorption capacity of Ce/Zr-MOF-808 increased sharply and rapidly reached its peak, suggesting a type I adsorption isotherm characteristic typical of a microporous structure. In the relative pressure region of 0.1 – 0.9, the adsorption capacity increased gradually, indicating the presence of mesoporous structure. Consequently, an H4 hysteresis loop appeared in the relative pressure region of 0.8 – 1.0, attributed to capillary condensation of N_2 within the mesopores [38]. In the relative pressure region of 0.9 – 1.0, the adsorption capacity rose sharply, revealing the existence of macropores in the material. The mesopores were probably formed by the accumulation of particles. According to the pore size distribution shown in Fig. 1d, the most probable ore size of Ce/Zr-MOF-808 was 1.7 nm, which was close to the characteristic micropore size of perfect MOF-808 [18]. As shown in Table S1, Ce/Zr-MOF-808 exhibited a specific surface area of 988.83 m^2/g. It was lower than that reported in the precious works [13, 18, 39]. However, Ce/Zr-MOF-808 exhibited both microporous and mesoporous structure, and higher average pore size of 2.2 nm. The former was conducive to the passage of dehydrating agent and promote the rate of dehydration [40], and the latter could provide highly accessible active sites for reactants [13, 18].

The results in Figs. 1c and 1d, and Table S1 further indicated that the recovered Ce/Zr-MOF-808 exhibited similar N_2 adsorption-desorption isotherms and pore size distribution to the fresh Ce/Zr-MOF-808. Moreover, the pore volume decreased only from 0.417 cm^3/g to 0.386 cm^3/g, suggesting that the structure of Ce/Zr-MOF-808 was only minimally affected during the reaction process. However, both the specific surface area and the average pore size decreased significantly. The former decreased to 511.01

m^2/g, and the latter dropped to 1.9 nm. This may be attributed to the deposition of insoluble carbon-containing compounds on the catalyst surface [41], as indicated by the FTIR shown in Fig. 1a. This could adversely affect the cyclic catalytic performance of Ce/Zr-MOF-808.

Figures 1e and 1f show the TGA and DTG curves of Ce/Zr-MOF-808 and its recovered sample after four cycles. The TGA curve of Ce/Zr-MOF-808 indicated that its mass loss can be divided into three stages [42]. The significant 21.7 wt% mass loss below 200 ℃ primarily originated from the desorption of physically adsorbed water. In the range of 200 to 400 ℃, the pronounced 19.3 wt% mass loss was attributed to the decomposition of − COO groups coordinated to metal node [18]. Within the 400–660 ℃ range, the 10.1 wt% mass loss stems from structural collapse of the catalyst and the breaking of coordination bonds between BTC and the metal center [18]. Above 660 ℃, only minor weight loss was observed, with the residue primarily composed of ZrO_2 and CeO_2 [42], accounting for approximately 47 wt%. The DTG curve of Ce/Zr-MOF-808 (Fig. 1f) revealed three distinct thermal degradation peaks at 103 ℃, 323 ℃, and 574 ℃, corresponding to the volatilisation of physically adsorbed water in the pores, the removal of −COOH and BTC, respectively.

The weight loss of the recovered Ce/Zr-MOF-808 also exhibited three distinct stages (Fig. 1e), but the extent of weight loss was significantly reduced compared to the fresh catalyst. Below 200 ℃, the mass loss rate decreased to 14.29 wt%, attributed to reduced physical adsorption water within the pores. This reduction likely resulted from decreased pore volume in the recycled catalyst, as evidenced by the N_2 adsorption-desorption isotherms shown in Fig. 1c. Within the temperature ranges of 200–450 ℃ and 450–660 ℃, mass losses of 13.7% and 18.1%, respectively, were detected due to the decomposition of the skeleton structure. Compared with the fresh catalyst, the maximum thermal degradation peaks of the recovered Ce/Zr-MOF-808 changed significantly (Fig. 1f). The decomposition temperature of −COOH increased from 323 to 422 ℃, which can be attributed to the enhanced crystallinity of the recycled catalyst (Fig. 1b), thereby improving the thermal stability [43]. Results in Figs. 1e and 1f indicated that Ce/Zr-MOF-808 exhibited good stability below 200 ℃, suggesting it is expected to demonstrate excellent catalytic stability during the conversion of CO_2 to DMC, typically conducted within the range from 120 to 150 ℃.

3.1.2 Catalyst morphology

Figure 2 shows the SEM images of Ce/Zr-MOF-808 and its recovered sample after four cycles. As shown in Fig. 2a, Ce/Zr-MOF-808 exhibited the structure characteristic of the MOF-808 base material, appearing as uniformly inter-grown irregular particles [18]. The mesopores were probably formed by the accumulation of particles Fig. 2b shows that the recovered Ce/Zr-MOF-808 exhibited a similar morphology to that of the fresh catalyst. These results indicate minimal structural changes in the catalyst during the reaction process, consistent with the XRD results shown in Fig. 1a. However, Fig. 2b also shows that the octahedron surface became rough after the reaction. This is attributed to the deposition of insoluble carbon-containing compounds on the catalyst surface during the reaction [21], as

confirmed by the FTIR and the N_2 adsorption-desorption isotherms shown in Figs. 1a and 1c. This phenomenon may adversely affect the cycling performance of Ce/Zr-MOF-808.

3.1.3 Catalyst composition characterization

Ce/Zr-MOF-808 was characterized by XPS, with results shown in Fig. S1 and Fig. 3a. In the XPS survey spectrum of Ce/Zr-MOF-808 (Fig. S1), characteristic peaks of O1s, C1s, Zr3d and Ce3d were observed, indicating the presence of O, C, Zr, and Ce elements in the catalyst. As depicted in Fig. 3a, three peaks at 531.8, 530 and 529.0 eV appeared in the XPS deconvoluted spectrum of O1s. Among them, 531.8 eV belonged to the binding energy of O in BTC ligand [24], while 530 and 529.0 eV were attributed to the binding energies of metal-coordinated O and electron-rich bridge – OH groups [24, 44], respectively. The presence of coordination O further confirmed the coordination interaction between – COO with metal centers. In the XPS spectrum of Zr3d, the peaks at 185.1 and 182.7 eV corresponded to $Zr3d_{3/2}$ and $Zr3d_{5/2}$, respectively [45], indicating that Zr completely coordinated and existed solely as Zr^{4+} in Ce/Zr-MOF-808. In the Ce 3d spectrum, the peaks at 885.3 and 880.6 eV belonged to Ce^{3+}, while those at 898.7, 888.9 and 882.5 eV belonged to Ce^{4+} [24], indicating that metal Ce existed in a mixed-valence of Ce^{3+} and Ce^{4+}. This further confirmed that Ce^{3+} underwent an electron loss process and combined with oxygen in the air to form CeO_2 during the formation of Ce/MOF-808, consistent with FTIR and XRD results shown in Fig. 1. The mixed form of Ce^{3+} and Ce^{4+} can synergistically activate CO_2 and CH_3OH through the generation of oxygen vacancies and redox cycle, thus playing a positive role in the formation of DMC.

XPS results showed that the Zr and Ce contents on the catalyst surface were 5.22% and 0.76%, respectively, revealing a molar ratio of Zr/Ce of 7:1. This represents a significant deviation from the 3:1 Zr/Ce molar ratio used in the catalyst preparation, indicating relatively low Ce content on the catalyst surface. The surface Ce species must be derived from both the exposed Ce metal centers in the skeleton of MOF and surface CeO_2. Consequently, the content of CeO_2 on the catalyst surface is extremely low. Since the catalytic activity is directly affected by the number of active components [11], revealing that the influence of CeO_2 on the performance and stability of Ce/Zr-MOF-808 is negligible.

The EDS energy dispersive spectrum and mapping spectra of Ce/Zr-MOF-808 are shown in Fig. S2 and Fig. 3b, respectively. Fig. S2 indicated that Ce/Zr-MOF-808 contained elements including O, Zr, and Ce, further confirming the successful preparation of the bimetallic catalyst. Additionally, the detected molar ratio of Ce to Zr in Ce/Zr-MOF-808 was 1:54,which was significantly lower than the bulk ratio of 1:1.59 determined by ICP-OES (Table S2), further suggesting a relatively low CeO_2 content on the catalyst surface and Ce preferentially entered the framework rather than existed as an uncoordinated species during the synthesis process, forming a bimetallic MOF in the framework. The mapping spectrum revealed uniform distribution of O, Zr and Ce within the catalyst (Fig. 3b), suggesting that this catalyst may exhibit favorable catalytic performance. Figures 1a and 1b showed that the detachment of CeO_2

was relatively easy to occur. However, it may have a negligible impact on the performance and stability of the catalyst due to its low amount.

To reveal the distribution of acidic and basic sites in Ce/Zr-MOF-808, NH_3-TPD and CO_2-TPD profiles were recorded, with results shown in Figs. 3c and 3d. In the NH_3-TPD profile of Ce/Zr-MOF-808, a desorption peak appeared at 158 ℃, which was caused by the acidic sites originated from Ce^{3+} and Zr^{4+} [18, 46], with a total acidity of 4.55 mmol/g.cat. In the CO_2-TPD profile of Ce/Zr-MOF-808 (Fig. 3d), the desorption peaks at 140 ℃ was attributed to basic sites originated from Zr − O, Ce − O in Zr/Ce clusters and unsaturated O^{2-} anion in Zr–O–Ce, Zr–O–Zr and Ce–O–Ce [13, 18], with a total basicity of 1.14 mmol/g. The results of NH_3-TPD and CO_2-TPD indicated that Ce/Zr-MOF-808 exhibited amphoteric catalytic properties with both acidic and basic active sites. Since the acid-base sites can play important roles for the direct synthesis of DMC from CO_2 and CH_3OH [14, 15], Ce/Zr-MOF-808 was expected to demonstrate outstanding catalytic performance.

3.2 Conversion of CO_2 to DMC

3.2.1 Screening of catalyst

The catalytic performance of common MOF materials such as UiO-66 and MOF-808 was first investigated, with results shown in Table 1. When using UiO-66 as the catalyst, only 0.05% DMC yield was obtained. However, in the presence of MOF-808, the DMC yield increased to 0.25%. This can be attributed to a larger specific surface area and oxygen vacancies of MOF-808, which enhanced the interaction between catalyst and substrate, promoting the activation of CO_2 and CH_3OH [47]. Further studies were conducted on the catalytic performance of doped MOF materials. As shown in Table 1, both the conversion of CH_3OH and yield of DMC increased after Ce doping. Using Ce/Zr-UiO-66 as the catalyst, the CH_3OH conversion and DMC yield were 0.35% and 0.3%, respectively, whereas under Ce/Zr-MOF-808, giving 0.44% and 0.36%. The enhanced catalytic activity of Ce-doped MOF materials arised from three factors. First, the introduction of Ce increased the number of Lewis acid/base active sites on the catalyst surface [13]. Second, the introduction of Ce resulted in MOF material with larger average pore size [48], which is also beneficial for the activation of reaction substrates, thus promoting the formation of CH_3O^- and CH_3^+ [18]. Third, the coexistence of Ce^{3+} and Ce^{4+} promoted the formation of oxygen vacancies, which can synergize with Zr^{4+} to enable the dual activation of CO_2 and CH_3OH. The catalytic performance of bimetal-doped MOF materials was also investigated. Compared to UiO-66 and MOF-808, both the conversion of CH_3OH and yield of DMC were slightly improved, giving 0.15% and 0.13%, and 0.29% and 0.24% in the presence of $Ce_{0.9}Ni_{0.1}$-UiO-66 and $Ce_{0.9}N_{i0.1}$-MOF-808, respectively. However, the catalytic activity of bimetal-doped MOF materials was lower than that of Ce-doped MOF catalyst. This can be attributed to the lower activity of Ni center compared to Ce metal center [49]. Since Ce-doped MOF-808 exhibited better catalytic performance, it was used for further investigation.

Table 1
Conversion of CO_2 to DMC over MOF-based catalysts.

Entry	Catalyst	CH_3OH conversion (%)	DMC selectivity (%)	DMC yield (%)
1	UiO-66	0.05	100.0	0.05
2	MOF-808	0.28	89.3	0.25
3	Ce/Zr-UiO-66	0.35	85.7	0.30
4[a]	Ce/Zr-MOF-808	0.44	81.8	0.36
5	$Ce_{0.9}Ni_{0.1}$-UiO-66	0.15	86.7	0.13
6	$Ce_{0.9}Ni_{0.1}$-MOF-808	0.29	82.7	0.24

Reaction conditions: 8 mL (200 mmol) CH_3OH, 0.25 g catalyst, 11 MPa CO_2, reaction temperature 150 °C, reaction time 12 h.

[a] Metal center : ligand (*n*:*n*) = 4:1, Ce:Zr (*n*:*n*) = 1:3.

3.2.2 Catalytic performance of Ce/Zr-MOF-808

The regulator provides the possibility to construct MOF materials with different structures [50], hence several common regulators such as PA, LA and FA were employed. The conversion of CO_2 to DMC was investigated in the presence of MOF materials derived from various regulators, with results shown in Fig. 4a. When BA was used as the regulator, almost no DMC production was detected, which can be attributed to the difficulty in forming a complete MOF framework under BA action [51]. In the presence of LA, the CH_3OH conversion rate was only 0.26%, and the DMC yield was merely 0.18%. This can be attributed to the molecular volume and weak coordination ability of LA, which resulted in fewer catalytic active centers [52]. When FA was employed as the regulator, Ce/Zr-MOF-808 possessed better catalytic performance, achieving 0.44% conversion of CH_3OH and 0.36% yield of DMC. Since FA can effectively regulate the coordination reaction between BTC and the metal center, thereby promoting the growth of MOF-808 crystals and the formation of a complete framework structure [53]. Furthermore, FA can also create the crystal defects, which facilitate direct contact between the substrate and active center [52]. Consequently, a higher yield of DMC was observed.

Further investigations were conducted on the effect of the molar ratio of ligand BTC to the metal center on the conversion of CO_2 to DMC, with results shown in Fig. 4b. With increasing the dosage of BTC, the conversion of CH_3OH, selectivity and yield of DMC initially increased before decreasing. As the amount of BTC increased, the collision probability between metal ions and BTC rose accordingly, leading to enhanced coordination between the metal center and BTC [54]. This, in turn, improves the crystallinity of MOF-808 and the stability of the catalyst [52]. Therefore, when the molar ratio of BTC to metal center increased from 1:5 to 1:4, catalytic performance improved. The conversion of CH_3OH, selectivity and

yield of DMC were 0.44%, 81.82% and 0.36%, respectively, with 1:4 molar ratio of BTC to metal center. However, with further increasing the amount of BTC, the conversion of CH_3OH, selectivity and yield of DMC all exhibited a decreasing trend. When the molar ratio of BTC to metal center was raised to 1:1, the conversion of CH_3OH, selectivity and yield of DMC decreased to 0.36%, 38.89% and 0.14%, respectively. Excess BTC interfered with the normal coordination between the metal center and BTC, leading to incomplete connection of the MOF skeleton and/or the formation of an amorphous structure [55]. Correspondingly, the catalytic performance declined.

The effect of Ce/Zr molar ratio on the conversion of CO_2 to DMC was also investigated, with results shown in Fig. 4c. As the Ce/Zr molar ratio increased, the conversion of CH_3OH and the yield of DMC first rose and then decreased, while the DMC selectivity remained relatively stable within the range of 75% to 90%. When the molar ratio of Ce to Zr increased from 1:4 to 1:3, the CH_3OH conversion increased slightly from 0.41% to 0.44%, while the DMC yield increased from 0.33% to 0.36%, respectively. The doping of suitable amount Ce in MOF-808 Ce increased the number of Lewis acid active sites in the catalyst, which is considered to favor the activation of CH_3OH to produce CH_3O^- and CH_3^+ [13]. In addition, Fig. S3a showed that Ce/Zr-MOF-808 derived from various Ce/Zr molar ratios exhibited similar FTIR spectra with slight differences in the intensity of characteristic bands. As the Ce/Zr molar ratio increased from 1:4 to 2:1, the intensity of the band at 660 cm^{-1} ascribed to the stretching vibration of Ce–O first increased and then decreased, reaching its maximum intensity at a Ce/Zr molar ratio of 1:3. The better catalytic performance of Ce/Zr-MOF-808 with 1:3 molar ratio of Ce to Zr can be attributed to the most abundant Ce – O bond derived from the coordination of Ce^{3+} and – COO. As the Ce/Zr molar ratio further increased, the DMC yield gradually decreased. When the Ce/Zr molar ratio reached 2:1, the conversion of CH_3OH and the yield of DMC dropped to 0.28% and 0.21%, respectively. This can be attributed to the reduction in Zr centers within Ce/Zr-MOF-808, as the interaction between Ce and Zr weakened with increasing Ce/Zr molar ratio [13]. Furthermore, as shown in the XRD patterns in Fig. S3b, the crystallinity of Ce/Zr-MOF-808 decreased with increasing Ce content in the catalyst, leading to reduced catalyst stability [24]. Collectively, these factors contribute to the decline in catalytic performance.

The effect of Ce/Zr-MOF-808 dosage on the catalytic conversion of CO_2 is shown in Fig. 4d. As the catalyst dosage increased, the conversion of CH_3OH and yield of DMC varied within the ranges of 0.36% to 0.44% and 0.28% to 0.36%, respectively, while the selectivity of DMC fluctuated slightly between 70% and 80%. When the catalyst dosage increased from 0.15 g to 0.25 g, the conversion of CH_3OH and yield of DMC increased from 0.39% to 0.44%, and 0.29% to 0.36%, respectively, which can be attributed to the increased availability of Lewis acid-base sites [11]. However, as the amount of Ce/Zr-MOF-808 was further increased, the DMC yield decreased. When the Ce/Zr-MOF-808 dosage reached 0.40 g, the conversion of CH_3OH and yield of DMC decreased to 0.36% and 0.28%, respectively. This can be attributed to excess catalyst hindering mass transfer, impeding substrate access to active sites, and thereby inhibiting equilibrium shift toward the target product formation [46].

3.2.3 Optimization of reaction system and conditions

The effects of common dehydrants such as MSs, TMM and 2-CP on the catalytic conversion of CO_2 to DMC were further investigated, with results shown in Fig. 5a. Both the conversion of CH_3OH and yield of DMC were significantly improved due to the addition of dehydrant. When MSs were used as the dehydrants, both CH_3OH conversion and DMC yield showed slight improvements, fluctuating within the ranges of 0.71% to 0.79% and 0.53% to 0.63%, respectively. Surprisingly, when 2-CP was employed as the dehydrant, the conversion of CH_3OH and selectivity of DMC were significantly improved to 1.28% and 92.19%, respectively. Since the H_2O generated during the reaction can be consumed by the hydration reaction of 2-CP [56], the reaction system advanced toward the formation of the target product, thereby enhancing the yield of DMC [57].

Based on the excellent dehydrating performance of 2-CP, its dosage effect on the catalytic conversion of CO_2 to DMC was also investigated, with results shown in Fig. 5b. As the 2-CP dosage increased, the conversion of CH_3OH and yield of DMC increased while the selectivity of DMC slightly changed in the range of 85% to 90%. When the molar ratio of 2-CP to CH_3OH was increased from 1:8 to 1:4, the conversion of CH_3OH rose from 1.38% to 2.83%, and the yield of DMC increased from 1.18% to 2.56%. However, further increase in the dosage of 2-CP led to decrease in the conversion of CH_3OH and yield of DMC. The conversion of CH_3OH and yield of DMC were 1.95% and 1.71% when the molar ratio of 2-CP to CH_3OH reached 1:3. This occurred because higher amounts of 2-CP promoted side reactions between 2-CP and CH_3OH, leading to the formation of methyl 2-pyridinecarboximidate (MPCI), which reduced DMC selectivity [3]. In addition, the solubility of CO_2 in 2-CP is lower than that in CH_3OH. The excessive dosage of 2-CP reduced the amount of CO_2 in the liquid phase, thereby hindering the contact of CO_2 with the catalyst.

Common reaction conditions such as reaction pressure, temperature and time were optimized, with results shown in Fig. S4. Since these reaction conditions affected the solubility of CO_2 in CH_3OH, catalyst structure, substrate activation, and side reactions [3, 20, 21, 58, 59], they were observed to significantly affect the catalytic conversion of CO_2. Under conditions of 10 MPa pressure and 140°C for 16 h, the CH_3OH conversion, DMC yield, and selectivity reached 5.56%, 94.24%, and 5.24%, respectively. The yield of DMC was higher than those obtained in the presence of the similar MOF materials including MOF-808, UiO-66 and their derivatives (Tables 1 and S3).

3.2.4 Recycling performance of Ce/Zr-MOF-808

After recovery, Ce/Zr-MOF-808 underwent cyclic catalytic performance testing, with results shown in Fig. 6a. Almost no change in the selectivity of DMC was observed while the conversion of CH_3OH and yield of DMC slightly decreased. After four cycles, the conversion of CH_3OH decreased from 5.56% to 4.54%, and the yield of DMC decreased from 5.24% to 4.13%, respectively. The results of FTIR (Fig. 1a), N_2 adsorption-desorption isotherms (Fig. 1c) and SEM (Fig. 2) results all confirmed that insoluble carbon-containing compounds deposited on the catalyst surface during the reaction, which led to the decrease in the specific surface area of catalyst and pore volume, thereby hindering substrate access to

the catalyst [41]. Additionally, the contents of Zr and Ce in the recovered catalyst after four cycles were also quantitatively analyzed by ICP-OES (Table S2). The Ce content decreased significantly from 19.61 to 16.13 wt%. Conversely, the Zr content increased from 20.26 to 24.69 wt%. These results revealed that the molar ratio of Ce to Zr in the recovered catalyst decreased from 1:1.59 in the fresh catalyst to 1:2.35. Therefore, it can be concluded that Ce was more susceptible to leaching during the reaction. This loss is likely associated with the removal of surface CeO_2 species, as corroborated by the FTIR and XRD results shown in Figs. 1a and 1b. The EDS energy spectrum of the recovered Ce/Zr-MOF-808 (Fig. S6a) indicated a molar ratio of Ce to Zr of 1:71 in the recovered catalyst. This value was significantly lower than that observed in fresh catalysts (1:54), further indicating that Ce detachment during the reaction primarily originated from CeO_2 on the catalyst surface. This finding was consistent with the FTIR and XRD results presented in Figs. 1a and 1b. Due to the catalytic activity of CeO_2 in the one-step synthesis of DMC from CO_2 and methanol [11], the shedding of CeO_2 also resulted in decrease in the conversion of CH_3OH and yield of DMC. However, owing to the extremely low CeO_2 content, its detachment had negligible impact on cyclic catalytic performance. Therefore, it can be considered that the deposition of the insoluble carbon-containing compounds on the catalyst surface was the primary cause of the decline in cyclic catalytic performance.

Based on the elemental-mapping of Ce/Zr-MOF-808 recovered after four cycles (Fig. S5), the spatial distributions of Ce, Zr and O remained uniform. Combined with the FTIR, XRD, N_2 adsorption-desorption, TGA and SEM results shown in Figs. 1 and 2, these findings indicated that Ce/Zr-MOF-808 maintained excellent structural stability throughout the reaction process. Consequently, even after four cycles, the DMC yield remained at 78.8% of the fresh catalyst yield, exhibiting only a slight decrease from 5.24% to 4.13%, as illustrated in Fig. 6a.

To evaluate the stability of Ce/Zr-MOF-808, leaching tests were conducted to confirm the loss of active components [25], with results shown in Fig. 6b. After reacting for 5 h in the presence of Ce/Zr-MOF-808, 2.31% yield of DMC was observed. Subsequently, the reaction was continued for another 11 h without the catalyst, resulting in a slight increase to 2.90%. This value was significantly lower than the yield of 5.24% achieved with Ce/Zr-MOF-808 over the entire 16 h catalytic period. These results indicated that the reaction of CO_2 with CH_3OH was significantly hindered after the removal of Ce/Zr-MOF-808, suggesting insignificant loss of its active components and excellent stability.

As described above, the decline in the cycling performance of Ce/Zr-MOF-808 can be attributed to the deposition of carbon-containing compounds on the catalyst surface and the detachment of CeO_2. Therefore, after removing Ce/Zr-MOF-808, the reaction was continued by adding a small amount of CeO_2, with the results shown in Fig. 6b. The addition of CeO_2 only slightly improved the conversion of CH_3OH and yield of DMC. When 0.15 g of CeO_2 was added, the conversion of CH_3OH increased from 3.16% to 3.60%, and the yield of DMC increased from 2.90% to 3.27%. These results indicated that CeO_2 on the catalyst surface promoted DMC formation, thereby CeO_2 detachment was one of the reasons for the decline in catalytic performance. However, even after adding CeO_2, both the conversion of CH_3OH

and yield of DMC were significantly lower than those (5.56% and 5.24%) obtained in the presence of Ce/Zr-MOF-808. Thus, it is reasonable to infer that the free CeO_2 did contribute to catalytic activity but its influence was relatively minor, and the catalytic activity mainly depended on Ce-Zr bimetallic sites in the skeleton. That is, Ce/Zr-MOF-808 played the predominant role in the catalytic reaction, in which the coexistence of Ce^{3+}/Ce^{4+} promoted the formation of oxygen vacancies, and there was a synergistic effect between Zr^{4+} (Lewis acid sites) and oxygen vacancies (basic sites).

3.3 Plausible mechanism for the conversion of CO_2 and CH_3OH to DMC

3.3.1 Product distribution for the direct synthesis of DMC from CO_2 over Ce/Zr-MOF-808

The reaction solution was subjected to qualitative analysis via gas chromatography-mass spectrometry (GC-MS). The total ion flow chromatogram was shown in Fig. S6, and the product distribution was listed in Table S4. In addition to the target product DMC, several byproducts were detected, including 2-picolinamide (2-PA), methyl 2-picolinate (MP) and MPCI. All these byproducts originated from 2-CP, with 2-PA being generated through the hydration reaction of 2-CP with H_2O. Since both 2-PA and 2-CP can react with CH_3OH to generate MP and MPCI, respectively, the selectivity for DMC decreased when 2-CP was in excess, as shown in Fig. 5b.

3.3.2 Investigation on the roles of acid-base sites of Ce/Zr-MOF-808

To elucidate the roles of acid-base sites for the direct synthesis of DMC from CO_2 and methanol catalyzed by Ce/Zr-MOF-808, Py and BA were further added to the reaction system. The results in Table 2 indicated that both the conversion of CH_3OH and yield of DMC significantly decreased upon the addition of Py and BA. Based on CO_2-TPD and NH_3-TPD results, Ce/Zr-MOF-808 was an amphoteric catalyst with acid-base active sites. After adding Py and BA, both the acid-base sites of the catalyst were occupied, thus resulting in a decrease in the catalytic activity. When 0.6 mmol Py was added to the reaction system, the conversion of CH_3OH and yield of DMC decreased from 5.56% to 4.53% and 5.24% to 3.88%, respectively. This can be attributed to Py adsorption on the acidic sites of the catalyst, which hindered the activation of CH_3OH. Therefore, the formation of intermediates including CH_3^+ and CH_3O^- was hindered [13], leading to a decrease in DMC yield. Furthermore, the presence of Py also hindered the adsorption of 2-CP on acid sites, diminishing its dehydration capability and impeding the formation of DMC [40]. Similarly, when BA was added, it was adsorbed on the basic sites of the catalyst, hindering the activation of CO_2 and the formation of intermediate CH_3OCOO^- [18]. When 0.15 mmol BA was added to the reaction system, the conversion of CH_3OH and yield of DMC decreased to 3.94% and 3.48%, respectively. The results of CO_2-TPD and NH_3-TPD indicated that the acid-base amounts of Ce/Zr-MOF-

808 were 4.55 and 1.14 mmol/g, respectively. That is 1.13 mmol acidic sites and 0.28 mmol basic sites were contained in 0.25 g catalyst. Therefore, when 1.2 mmol Py or 0.3 mmol BA was added to the system, the acidic or basic sites of Ce/Zr-MOF-808 were completely occupied. Correspondingly, the conversion of CH_3OH and yield of DMC further decreased. The conversion of CH_3OH and yield of DMC decreased to 2.41% and 1.96% in the presence of the former, and the conversion of CH_3OH and yield of DMC decreased to 3.12% and 2.67% in the presence of the latter. As shown in Table 2, when acidic sites were fully occupied, the decrease in the conversion of CH_3OH and yield of DMC was more pronounced, indicating that acidic sites played a dominant role in the direct synthesis of DMC from CO_2 and CH_3OH. Furthermore, after adding Py and BA, both the selectivity of DMC decreased significantly. These results indicated that both the reduction in acid sites and base sites led to decrease in the selectivity of DMC, revealing a synergistic effect between them. When the acidic sites were fully occupied, the decline in DMC selectivity was more pronounced, further confirming that acidic sites played the dominant role during the reaction process.

Table 2
Effect of additive on the conversion of CO_2 and CH_3OH to DMC.

Entry	Additive/amount (mmol)	CH_3OH conversion (%)	DMC selectivity (%)	DMC yield (%)
1	/	5.56	94.24	5.24
2	Py/0.6	4.53	85.65	3.88
3	Py/1.2	2.41	81.33	1.96
4	BA/0.15	3.94	88.32	3.48
5	BA/0.3	3.12	85.58	2.67

Reaction conditions: FA as regulator, metal center:ligand = 4:1, Ce:Zr = 1:3, 0.25 g Ce/Zr-MOF-808, 8 mL CH_3OH, 2-CP:CH_3OH = 1:4, 10 MPa CO_2, reaction temperature 140 °C, reaction time 16 h.

3.3.3 In situ FTIR

The adsorption of CH_3OH and CO_2 on Ce/Zr-MOF-808 was characterized by *in situ* FTIR, and the results are shown in Fig. 7. In Fig. 7a, the broad absorption band at 2945 cm^{-1} is attributed to the stretching vibration of the C–H bond in CH_3OH. Additionally, the characteristic absorption bands attributed to the intermediates CH_3^+ and CH_3O^- also appeared. The bans at 2877 and 2823 cm^{-1} are caused by the bending vibration and the asymmetric stretching vibration of the C–H bond in CH_3^+ and CH_3O^- [18, 60], respectively. The bands at 1133 and 1020 cm^{-1} are attributed to the bending vibration and stretching vibration of the C–O bond in CH_3O^- [60]. These results indicated that CH_3OH can be simultaneously activated to CH_3^+ and CH_3O^- over Ce/Zr-MOF-808. After the introduction of CO_2, the intensities of the bands at 2823, 1133 and 1020 cm^{-1} belonged to the intermediate CH_3O^- was significantly weakened,

while the band at 1488 cm^{-1} corresponded to the intermediate CH_3OCOO^- appeared [60], indicating that CH_3O^- can combine with CO_2 to form the intermediate CH_3OCOO^-. These results indicated that the intermediates of CH_3^+, CH_3O^- and CH_3OCOO^- during the direct synthesis of DMC from CO_2 over Ce/Zr-MOF-808.

3.3.4 Reaction mechanism for the direct synthesis of DMC from CO_2 over Ce/Zr-MOF-808

Based on the results obtained from this work and previously reported works [9, 18, 24, 40], a plausible reaction mechanism for the direct synthesis of DMC from CO_2 catalyzed by Ce/Zr-MOF-808 was further proposed, in which six steps are contained, as shown in Fig. 8. First, two molecules of CH_3OH were adsorbed by Ce/Zr-MOF-808. One molecule of CH_3OH was adsorbed by metal sites of Ce^{3+} and activated to form methyl cation (CH_3^+) and OH^-. The other molecule of methanol released hydrogen ions (H^+) and formed methoxy anions (CH_3O^-) under the action of metal sites of Zr^{4+}. CH_3^+ was further adsorbed on the oxygen vacancy to generate a bridged methoxy [Zr–(OCH_3) – Ce] (step 1). Secondly, 2-CP was adsorbed on Ce^{3+} sites, and a 2-PA adsorption resonance structure was derived from – OH and 2-CP (step 2). Thirdly, the 2-PA adsorption resonance structure combined with H^+ to form 2-PA, after which this structure detached and exposed oxygen vacancy (step 3). Subsequently, CO_2 was activated at the oxygen vacancy (step 4). The activated CO_2 was combined with CH_3O^- to form the intermediate CH_3OCOO^- (step 5). Ultimately, the intermediate CH_3OCOO^- reacted with CH_3^+ released from $Ce^-(OCH_3)^-Zr$ to generate DMC (step 6).

4 Conclusion

An efficient and stable Ce-doped Zr-MOF-808 catalyst with bimetallic centers was developed for the direct synthesis of DMC from CO_2 and CH_3OH. The catalyst was simply prepared by one-pot method, and it still possessed the characteristic structure of Zr-based MOF-808. Ce/Zr-MOF-808 contained both Lewis acid-base sites and coexisting Ce^{3+}/Ce^{4+} species. Ce doping enhanced the catalytic performance, Ce/Zr-MOF-808 exhibited superior activity compared to the similar MOF materials including MOF-808, UiO-66 and their derivatives. The conversion of CH_3OH and yield of DMC reached 5.56% and 5.24%, respectively. The structure of Ce/Zr-MOF-808 also remained well during the reaction, and the loss of active components was insignificant. After four cycles, the conversion of CH_3OH and yield of DMC slightly decreased to 4.54% and 4.13%, respectively. The yield of DMC still retained 78.8% of the initial activity. The decrease in the cyclic catalytic performance was primarily caused by the deposition of carbon-containing compounds on the catalyst surface and the loss of a small amount of CeO_2. A possible reaction mechanism for the direct synthesis of DMC from CO_2 and CH_3OH over Ce/Zr-MOF-808 was proposed, wherein both Lewis acid-base sites played important roles. The synergistic effect

between Zr^{4+} (Lewis acid sites) and Ce^{3+}/Ce^{4+}-induced oxygen vacancies (Lewis base sites) was responsible for the enhanced catalytic performance of Ce/Zr-MOF-808.

Declarations

Declaration of Competing Interest

The authors declare that they have no known competing financial interests or personal relationships that could have appeared to influence the work reported in this paper.

Appendix A. Supplementary data

Supplementary data to this article can be found online.

Author Contribution

C. L.: Data curation, Formal analysis, Investigation, Writing – original draft. -Y. Z.: Formal analysis, Investigation, Writing – original draft. -W. W.: Data curation, Investigation. -G. F.: Conceptualization, Funding acquisition, Methodology, Resources, Supervision, Writing – review & editing.

Acknowledgement

This work was financially supported by Project of Hubei Provincial Department of Education (Q20231601) and (D20241706).

Data Availability

Supplementary data to this article can be found online.

References

1. Z. Deng, B.Q. Zhu, S.J. Davis, P. Ciais, D. Guan, P. Gong, Z. Liu, Global carbon emissions and decarbonization in 2024. Nat. Rev. Earth Env. **6**, 231–233 (2025). https://doi.org/10.1038/s43017-025-00658-x
2. M. Zhang, Y. Xu, B.L. Williams, M. Xiao, S. Wang, D. Han, L. Sun, Y. Meng, Catalytic materials for direct synthesis of dimethyl carbonate (DMC) from CO. J. Clean. Prod. **279**, 123344 (2021). https://doi.org/10.1016/j.jclepro.2020.123344

3. Q.Y. Zhang, D. Zhang, W. Mao, D. Zhu, L. Liu, H. Liu, Y. Huang, H. Chen, X. Luo, Z. Liang, Synthesis of dimethyl carbonate from CO. methanol over Zn modified CeO2 2-cyanopyridine: Theoretical calculation Exp. Sep. Purif. Technol. **339**, 126217 (2024). https://doi.org/10.1016/j.seppur.2023.126217
4. A. Poungsombate, T. Imyen, P. Dittanet, B. Embley, P. Kongkachuichay, Direct synthesis of dimethyl carbonate from CO. methanol supported bimetallic Cu-Ni/ZIF-8 MOF catalysts J. Taiwan. Inst. Chem. E. **80**, 16–24 (2017). https://doi.org/10.1016/j.jtice.2017.07.019
5. Y. Wu, Research progress on catalysts for the direct synthesis of dimethyl carbonate from carbon dioxide and methanol. Chem. Eng. **37**, 79–82 (2023). https://doi.org/10.16247/j.cnki.23-1171/tq.20230479
6. A.H. Tamboli, A.A. Chaugule, H. Kim, Catalytic developments in the direct dimethyl carbonate synthesis from carbon dioxide and methanol. Chem. Eng. J. **323**, 530–544 (2017). https://doi.org/10.1016/j.cej.2017.04.112
7. D. Delledonne, F. Rivetti, U. Romano, Developments in the production and application of dimethylcarbonate. Appl. Catal. A-Gen. **221**, 241–251 (2001). https://doi.org/10.1016/S0926-860X(01)00796-7
8. X. Ma, S. Huang, S. Wang, P. Zhang, Advance in synthesis of organic carbonate by oxidative carbonylation. Petrochem. Technol. **30**, 697–705 (2010)
9. G. Hou, Q. Wang, D. Xu, H. Fan, K. Liu, Y. Li, K.X. Gu, M. Ding, Dimethyl carbonate synthesis from CO. over CeO2 electron-enriched lattice oxygen species Angew Chem. Int. Ed. **63**, e202402053 (2024). https://doi.org/10.1002/ange.202402053
10. S.K. Kabra, E. Turpeinen, R.L. Keiski, G.D. Yadav, Direct synthesis of dimethyl carbonate from methanol and carbon dioxide: A thermodynamic and experimental study. J. Supercrit Fluids. **117**, 98–107 (2016). https://doi.org/10.1016/j.supflu.2016.05.039
11. D. Shi, S. Heyte, M. Capron, S. Paul, Catalytic processes for the direct synthesis of dimethyl carbonate from CO. methanol: Rev. Green. Chem. **24**, 1067–1089 (2022). https://doi.org/10.1039/d1gc04093f
12. J. Yu, X. Gu, Y. Bai, S. Gao, Y. Yu, Research Progress in Dimethyl Carbonate Synthesis from CO. Methanol Catalyzed CeO2-based Catalyst Chem. Eng. Commun. **49**, 18–20 (2023). https://doi.org/10.3969/j.issn.1003-6490.2023.07.007
13. L. Huo, L. Wang, J.J. Li, Y. Pu, K. Xuan, C. Qiao, H. Yang, Cerium doped Zr-based metal-organic framework as catalyst for direct synthesis of dimethyl carbonate from CO. J. CO2. Util. **68**, 102352 (2023). https://doi.org/10.1016/j.jcou.2022.102352
14. K. Jung, A. Bell, An in situ infrared study of dimethyl carbonate synthesis from carbon dioxide and methanol over zirconia. J. Catal. **204**, 339–347 (2001). https://doi.org/10.1006/jcat.2001.3411
15. S. Xie, A. Bell, An in situ raman study of dimethyl carbonate synthesis from carbon dioxide and methanol over zirconia. Catal. Lett. **70**, 137–143 (2000). https://doi.org/10.1023/A:1018837317910

16. P. Kumar, P. With, V.C. Srivastava, R. Gläser, I.M. Mishra, Efficient ceria-zirconium oxide catalyst for carbon dioxide conversions: Characterization, catalytic activity and thermodynamic study. J. Alloy Compd. **696**, 718–726 (2017). https://doi.org/10.1016/j.jallcom.2016.10.293
17. J. Al-Darwish, M. Senter, S. Lawson, F. Rezaei, A.A. Rownaghi, Ceria nanostructured catalysts for conversion of methanol and carbon dioxide to dimethyl carbonate. Catal. Today. **350**, 120–126 (2020). https://doi.org/10.1016/j.cattod.2019.06.013
18. K. Xuan, Y. Pu, F. Li, J. Luo, N. Zhao, F. Xiao, Metal-organic frameworks MOF-808-X as highly efficient catalysts for direct synthesis of dimethyl carbonate from CO. methanol Chin. J. Catal. **40**, 553–566 (2019). https://10.1016/S1872-2067(19)63291-2
19. Y. Fan, H. Zhang, M. Ren, Y. Zhang, Y. Li, L. Wang, J. Chen, Low-temperature catalytic degradation of chlorinated aromatic hydrocarbons over bimetallic Ce-Zr/UiO-66 catalysts. Chem. Eng. J. **414**, 128782 (2021). https://doi.org/10.1016/j.cej.2021.128782
20. J. Zhao, Y. Zhang, K. Wang, C. Yan, Z. Da, C. Li, Y. Yan, Development of hierarchical porous MOF-based catalyst of UiO-66(Hf) and Its application for 5-hydroxymethylfurfural production from cellulose. Chem. Select. **3**, 11476–11485 (2018). https://doi.org/10.1002/slct.201802423
21. W. Zhang, J. Liu, H. Gu, C. Pan, Y. Long, Q. Cheng, G. Fan, Transfer hydrogenation of 5-hydroxymethylfurfural to 2,5-dihydroxymethylfuran by synergistic catalysis with a mixture of ZIF-8 and UiO-66-NH. Renew. Energy. **240**, 122148 (2025). https://doi.org/10.1016/j.renene.2024.122148
22. M. Honda, M. Tamura, Y. Nakagawa, S. Sonehara, K. Suzuki, K. Fujimoto, K. Tomishige, Ceria-catalyzed conversion of carbon dioxide into dimethyl carbonate with 2-cyanopyridine. ChemSusChem. **6**, 1341–1344 (2013). https://doi.org/10.1002/cssc.201300229
23. S. Wang, J. Zhou, S. Zhao, Y. Zhao, X. Ma, Enhancements of dimethyl carbonate synthesis from methanol and carbon dioxide: The in situ hydrolysis of 2-cyanopyridine and crystal face effect of ceria. Chin. Chem. Lett. **26**, 1096–1100 (2015). https://doi.org/10.1016/j.cclet.2015.05.005
24. L. Qian, J. Cheng, K. Xin, H. Guo, Y. Mao, J. Tu, W. Yang, Enhanced hydroxyl bridge-mediated microalgal lipid conversion via mixed-valence Ce/Zr-MOF-808 catalysts at reduced temperatures. Sustain. Energ. Fuels. **8**, 3304–3316 (2024). https://doi.org/10.1039/D4SE00647J
25. W. Chen, Q. Peng, G. Fan, Q. Cheng, M. Tu, G. Song, Catalytic transfer hydrogenation of furfural to furfuryl alcohol over Al-containing ferrihydrite. J. Ind. Eng. Chem. **119**, 574–585 (2023). https://doi.org/10.1016/j.jiec.2022.12.002
26. H. Zhao, H. Zhang, J. Wang, B. Li, Y. Zhu, H. Liu, Theoretical calculation and tests of hydrogen storage properties of Nano MoS. doped Ce/Zr-MOF-808 J. Energy Storage. **88**, 111526 (2024). https://doi.org/10.1016/j.est.2024.111526
27. M.C. Sánchez-Lemus, F.F. Schoeggl, S.D. Taylor, S.I. Andersen, M.M. Mapolelo, S.C. Mahavadi, H.W. Yarranton, Characterization of heavy distillation cuts using fourier transform infrared spectrometry: Proof of concept. Energy Fuels. **30**, 10187–10199 (2016). https://doi.org/10.1021/acs.energyfuels.6b01912

28. H.N. Abdelhamid, UiO-66 as a catalyst for hydrogen production via the hydrolysis of sodium borohydride. Dalton Trans. **49**, 10851–10857 (2020). https://doi.org/10.1039/D0DT01688H
29. B. Dang, D. Gao, Y. Luo, Z. Zhang, J. Li, F. Wu, Bifunctional design of cerium-based metal-organic framework-808 membrane modified separator for polysulfide shuttling and dendrite growth inhibition in lithium-sulfur batteries. J. Energy Storage. **52**, 104981 (2022). https://doi.org/10.1016/j.est.2022.104981
30. G. Yang, J. Li, Fabrication of profenofos electrochemical sensor by bimetal-organic framework MOF-808(Zr/Ce) with organophosphorus hydrolase-like activity. Chin. J. Anal. Chem. **51**, 1112–1121 (2023). https://doi.org/10.19756/j.issn.0253-3820.221636
31. J. Zhou, L. Xu, J. Sun, D. He, H. Jiao, Yolk-shell Au@CeO. microspheres: Synthesis application photocatalytic Degrad. methylene blue dye Surf. Coat. Tech. **271**, 119–126 (2015). https://doi.org/10.1016/j.surfcoat.2014.12.069
32. L. Valenzano, B. Civalleri, S. Chavan, S. Bordiga, M. Nilsen, S. Jakobsen, K.P. Lillerud, C. Lamberti, Disclosing the complex structure of UiO-66 metal organic framework: A synergic combination of experiment and theory. Chem. Mater. **23**, 1700–1718 (2011). https://doi.org/10.1021/cm1022882
33. G. Fan, Y. Chen, Y. Lu, Q. Cheng, B. Chai, G. Song, Co-production of 5-hydroxymethyl furfural and furfural from holocellulose over UiO-66-derived acid-base catalysts. Chem. Eng. Sci. **276**, 118768 (2023). https://doi.org/10.1016/j.ces.2023.118768
34. Z. Hu, Y. Peng, Z. Kang, Y. Qian, D. Zhao, A modulated hydrothermal (MHT) approach for the facile synthesis of UiO-66-Type MOFs. Inorg. Chem. **54**, 4862–4868 (2015). https://doi.org/10.1021/acs.inorgchem.5b00435
35. M. Yao, R.J. Baird, F.W. Kunz, T.E. Hoost, An XRD and TEM investigation of the structure of alumina-supported ceria-zirconia. J. Catal. **166**, 67–74 (1997). https://doi.org/10.1006/jcat.1997.1504
36. K. Ki-Joong, T.C. Jeffrey, R.O. Paul, K.T. Praveen, T. Jinhui, Synthesis of high-quality Mg-MOF-74 thin film via vapor-assisted crystallization. ACS Appl. Mater. Interfaces. **13**, 35223–35231 (2021). https://doi.org/10.1021/acsami.1c12000
37. Y. Wei, Y. Zhang, B. Li, C. Yan, Z. Da, M. Meng, C. Liu, Y. Yan, Fabrication of graphene oxide supported acid-base bifunctional metal-organic frameworks as efficient catalyst for glucose to 5-hydroxymethylfurfural conversion. Energy Technol. **8**, 1901111 (2020). https://doi.org/10.1002/ente.201901111
38. A. Dutta, D. Gupta, A. Patra, B. Saha, A. Bhaumik, Synthesis of 5-hydroxymethylfurural from carbohydrates using large-pore mesoporous tin phosphate. ChemSusChem. **7**, 925–933 (2014). https://doi.org/10.1002/cssc.201300766
39. J. Wang, Y. Zhang, J. Diao, J. Zhang, H. Liu, D. Su, A MoS. nanocatalyst surface-enriched Act. sites Heterogen. Transf. hydrogenation nitroarenes Chin. J. Catal. **39**, 79–87 (2018). https://doi.org/10.1016/S1872-2067(17)62925-5
40. H. Liu, D. Zhu, B. Jia, Y. Huang, Y. Cheng, X. Luo, Z. Liang, Study on catalytic performance and kinetics of high efficiency CeO. catalyst prepared freeze Dry. synthesis dimethyl carbonate CO2

methanol Chem. Eng. Sci. **254**, 117614 (2022). https://doi.org/10.1016/j.ces.2022.117614

41. H. Yang, X. Du, X. Lei, K. Zhou, Y. Tian, D. Li, C. Hu, Unraveling enhanced activity and coke resistance of Pt-based catalyst in bio-aviation fuel refining. Appl. Energy. **301**, 117469 (2021). https://doi.org/10.1016/j.apenergy.2021.117469
42. G. Shearer, S. Chavan, S. Bordiga, S. Svelle, U. Olsbye, K.P. Lillerud, Defect engineering: Tuning the porosity and composition of the metal-organic framework UiO-66 via modulated synthesis. Chem. Mater. **28**, 3749–3761 (2016). https://doi.org/10.1021/acs.chemmater.6b00602
43. H.U. Escobar-Hernandez, L.M. Pérez, P.F. Hu, F.A. Soto, M.I. Papadaki, H. Zhou, Q. Wang, Thermal stability of metal-organic frameworks (MOFs): Concept, determination, and model prediction using computational chemistry and machine learning. Ind. Eng. Chem. Res. **6**, 5853–5862 (2022). https://doi.org/10.1021/acs.iecr.2c00561
44. E. Moretti, L. Storaro, A. Talon, P. Riello, A.I. Molina, E. Rodríguez-Castellón, 3-D flower like Ce-Zr-Cu mixed oxide systems in the CO preferential oxidation (CO-PROX): Effect of catalyst composition. Appl. Catal. B-Environ. (2015). 168 – 169, 385 – 395. https://doi.org/10.1016/j.apcatb.2014.12.032
45. A.S. Abou-Elyazed, Y. Sun, A.M. El-Nahas, S. Abdel-Azeim, T.Z. Sharara, A.M. Yousif, Solvent-free synthesis and characterization of Ca. joint experimental Comput. study Mater. Today Sustain. **18**, 100110 (2022). https://doi.org/10.1016/j.mtsust.2022.100110
46. K. Xuan, F. Pu, F. Li, A. Li, J. Luo, L. Li, F. Wang, N. Zhao, F. Xiao, Direct synthesis of dimethyl carbonate from CO. J. CO2. Util. **27**, 272–282 (2018). https://doi.org/10.1016/j.jcou.2018.08.002
47. C. Simms, A. Mullaliu, F. Azambuja, G. Aquilanti, T.N. Parac-Vogt, Green, Safe, and Reliable Synthesis of Bimetallic MOF-808 Nanozymes With Enhanced Aqueous Stability and Reactivity for Biological Applications. Small. **20**, 2307236 (2023). https://doi.org/10.1002/smll.202307236
48. E. Geravand, F. Farzaneh, R. Gil-San-Millan, F.J. Carmona, J.A.R. Navarro, Mixed-metal cerium/zirconium MOFs with improved nerve agent detoxification properties. Inorg. Chem. **59**, 16160–16167 (2020). https://doi.org/10.1021/acs.inorgchem.0c01434
49. D. Stoian, F. Medina, A. Urakawa, Improving the stability of CeO. catalyst rare earth metal promotion Mol. insights dimethyl carbonate synthesis CO2 methanol 2-cyanopyridine ACS Catal. **8**, 3181–3193 (2018). https://doi.org/10.1021/acscatal.7b04198
50. S. Kang, M. Zhang, H. Zheng, Critical factors influencing the structures and properties of metalorganic frameworks. CrystEngComm. **17**, 981–991 (2015). https://doi.org/10.1039/C4CE02150A
51. T. Chen, H. Xu, S. Li, J. Zhang, Z. Tan, L. Chen, Y. Chen, Z. Huang, H. Pang, Tailoring the electrochemical responses of MOF-74 via dual-defect engineering for superior energy storage. Adv. Mater. **36**, 2402234 (2024). https://doi.org/10.1002/adma.202402234
52. L. Jin, C. Zhou, S. Chen, P. Liu, Controlled synthesis of defective MOF-808 and its application in levulinic acid esterification. Appl. Catal. Gen. **681**, 119773 (2024). https://doi.org/10.1016/j.apcata.2024.119773

53. Z. Hu, I. Castano, S. Wang, Y. Wang, Y. Peng, Y. Qian, C. Chi, X. Wang, D. Zhao, Modulator effects on the water-based synthesis of ZrHf metal-organic frameworks quantitative relationship studies between modulator, synthetic condition, and performance. Cryst. Growth Des. **16**, 2295–2301 (2016). https://doi.org/10.1021/acs.cgd.6b00076
54. Y. Su, Y. Zhang, W. Feng, G. Zhang, Y. Sun, Monocarboxylic acid structural analogues facilitate in situ composite of functional complexes for aqueous batteries. Angew Chem. Int. Ed. **64**, e202502752 (2025). https://doi.org/10.1002/anie.202502752
55. M. Lv, Synthesis of MOF-derived metal-nitrogen-carbon single-atom electrocatalysts and their oxygen reduction reaction properties. Dissertation of South China University of Technology, Guangzhou, (2022). https://doi.org/10.27151/d.cnki.ghnlu.2022.001826
56. W. Sun, P. Li, M. Yabushita, Y. Nakagawa, Y. Wang, A. Nakayama, K. Tomishige, Comparative study between 2-furonitrile and 2-cyanopyridine as dehydrants in direct synthesis of dialkyl carbonates from CO. alcohols over cerium oxide catalyst ChemSusChem. **16**, e202300768 (2023). https://doi.org/10.1002/cssc.202300768
57. H. Ohno, M. Ikhlayel, M. Tamura, K. Nakao, K. Suzuki, K. Morita, Y. Kato, K. Tomishige, Y. Fukushima, Direct dimethyl carbonate synthesis from CO. methanol catalyzed CeO2 Assist. 2-cyanopyridine: cradle-to-gate Greenh. gas emission study Green. Chem. **23**, 457–469 (2021). https://doi.org/10.1039/D0GC03349A
58. M. Honda, M. Tamura, Y. Nakagawa, K. Nakao, K. Suzuki, K. Tomishige, Organic carbonate synthesis from CO. alcohol over CeO2 2-cyanopyridine: Scope mechanistic Stud. J. Catal. **318**, 95–107 (2014). https://doi.org/10.1016/j.jcat.2014.07.022
59. P. Wang, Z. Wu, P. Emayavaramban, B. Yang, Oxidative cleavage of biomass model molecules catalyzed by Cu-Beta zeolite. J. Chem. Eng. Chin. Univ. **35**, 1010–1019 (2021). https://doi.org/10.3969/j.issn.1003-9015.2021.06.008
60. Y. Xia, C. Huang, J. Wang, G. Cai, M. Zhang, Synergistic effects of poly (ionic liquids)@MOF-808 nanocomposites for direct conversion of carbon dioxide into dimethyl carbonate. Langmuir. **41**, 32761–32769 (2025). https://doi.org/10.1021/acs.langmuir.5c04812
61. Y. Zhang, Q. Li, W. Feng, S. Gao, H. Yue, Regulating electron transfer in vanadium-based metal-organic frameworks via the synergy of linker engineering and machine learning for efficient and reversible aqueous zinc ion batteries. Adv. Mater. **37**, 2507609 (2025). https://doi.org/10.1002/adma.202507609
62. Y. Zhang, Q. Li, W. Feng, H. Yue, S. Gao, Y. Su, Y. Tang, J. Wu, Z. Zhang, Y. Zhang, M. Shakouri, H. Chen, H. Pang, Valence engineering via polyoxometalate-induced on vanadium centers for efficient aqueous zinc-ion batteries. Angew. Chem. Int. Edit. 137, e202501728 A(2025). https://doi.org/10.1002/ange.202501728

Figures

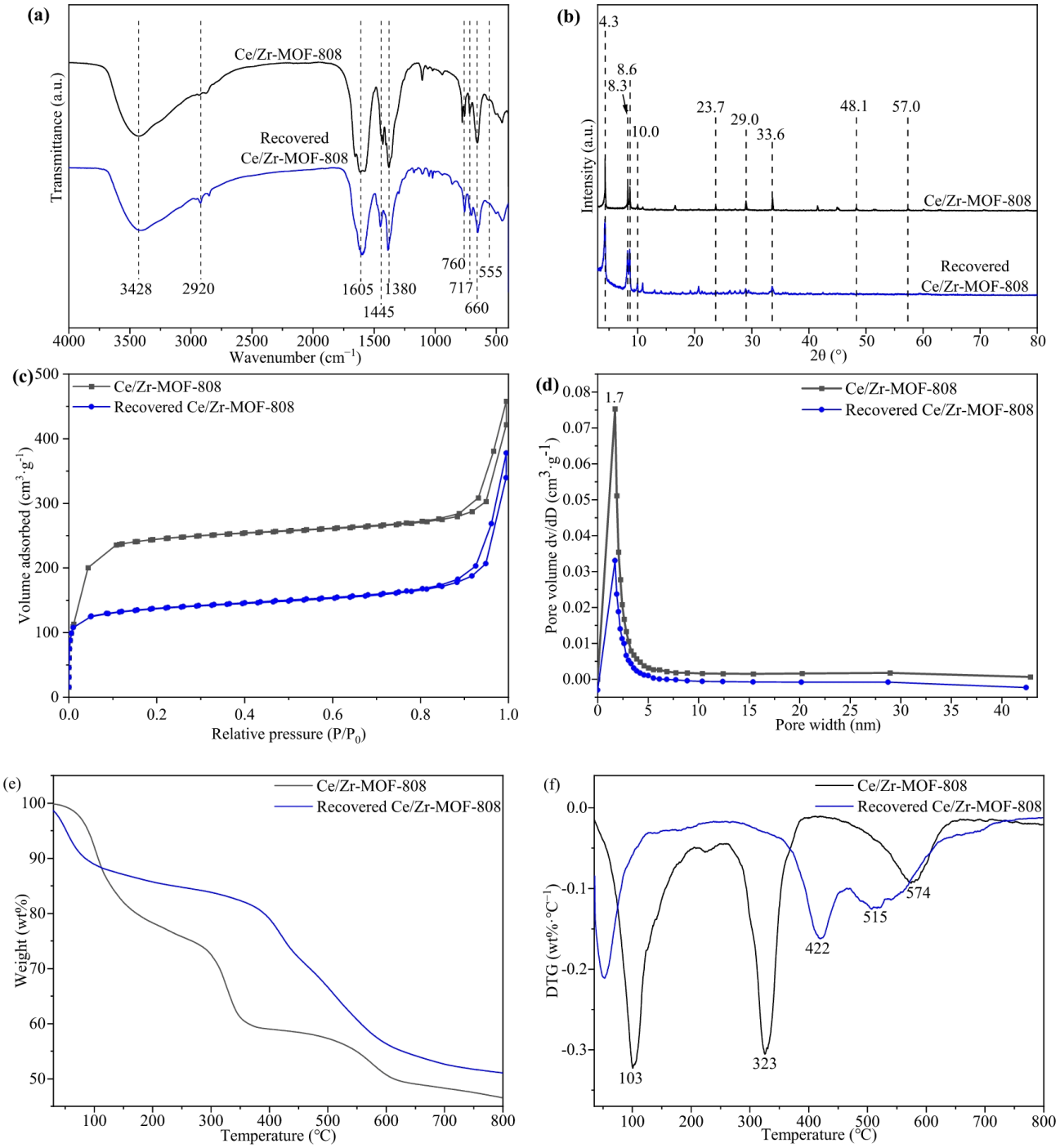


Figure 1

Structure characterization of Ce/Zr-MOF-808 (a) FTIR, (b) XRD, (c) N_2 adsorption-desorption isotherms, (d) pore size distributions, (e) TGA curves and (f) DTG curves.

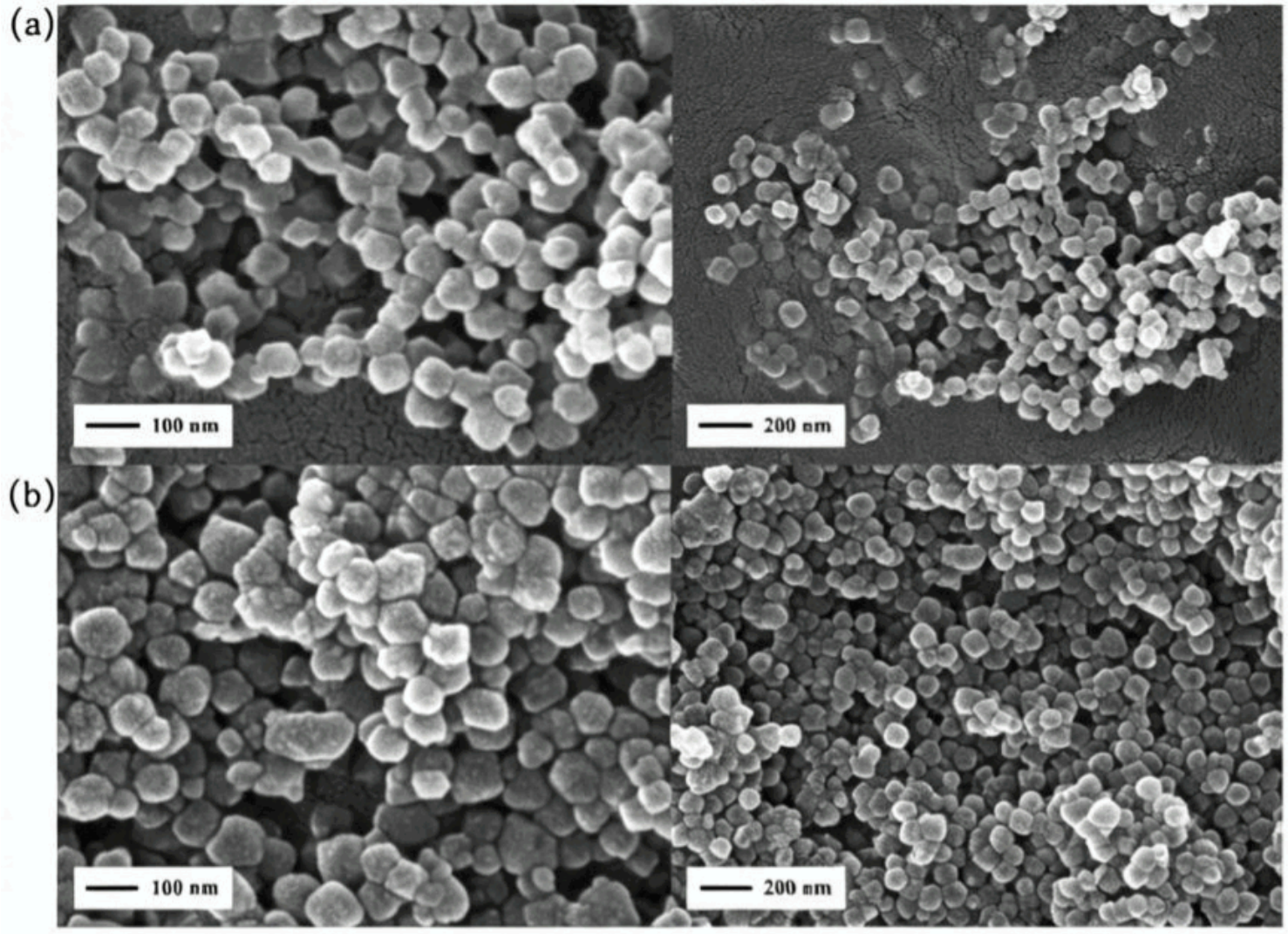


Figure 2

SEM images of (a) Ce/Zr-MOF-808 and (b) recovered Ce/Zr-MOF-808.

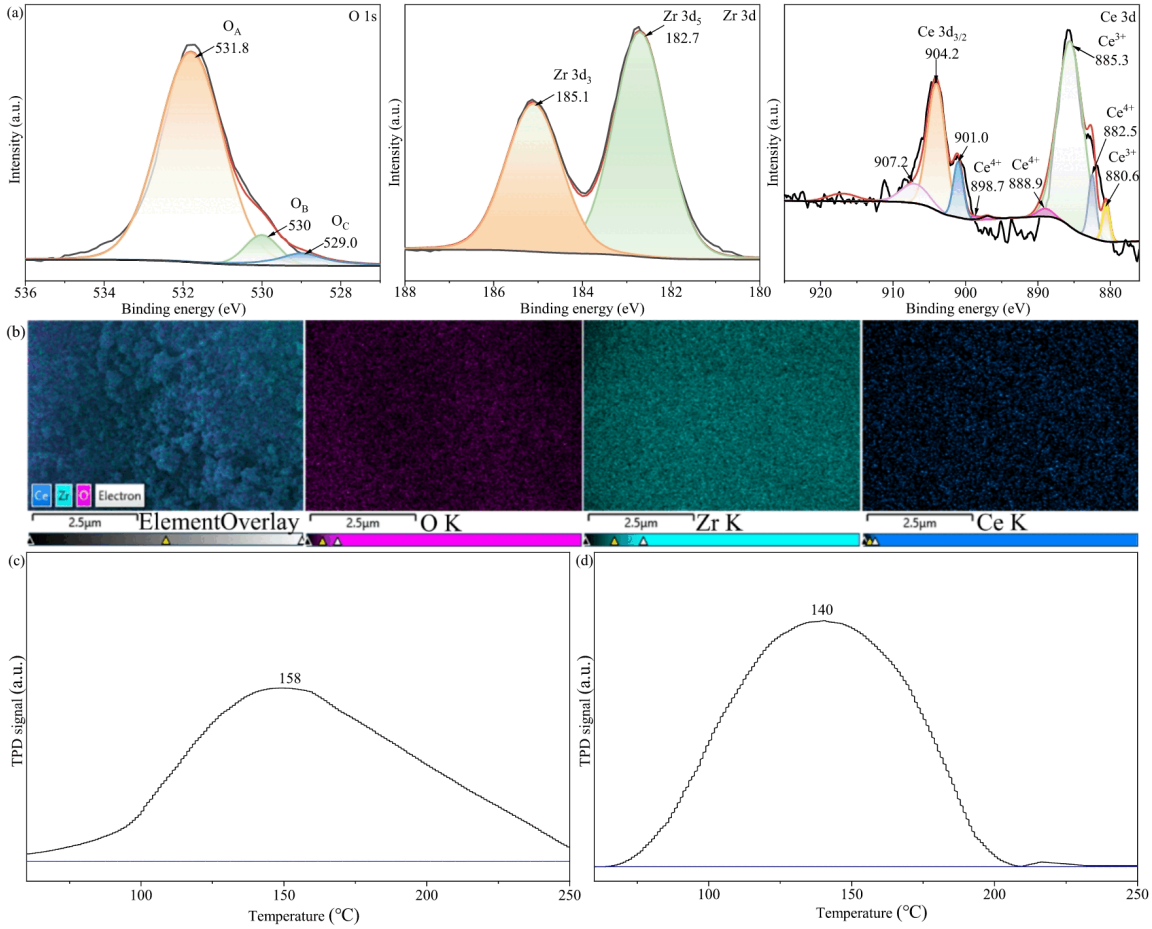


Figure 3

Composition characterization of Ce/Zr-MOF-808 (a) deconvoluted XPS spectra of O 1s, Zr 3d and Ce 3d, (b) mapping spectra, (c) NH_3-TPD profiles and (d) CO_2-TPD profiles.

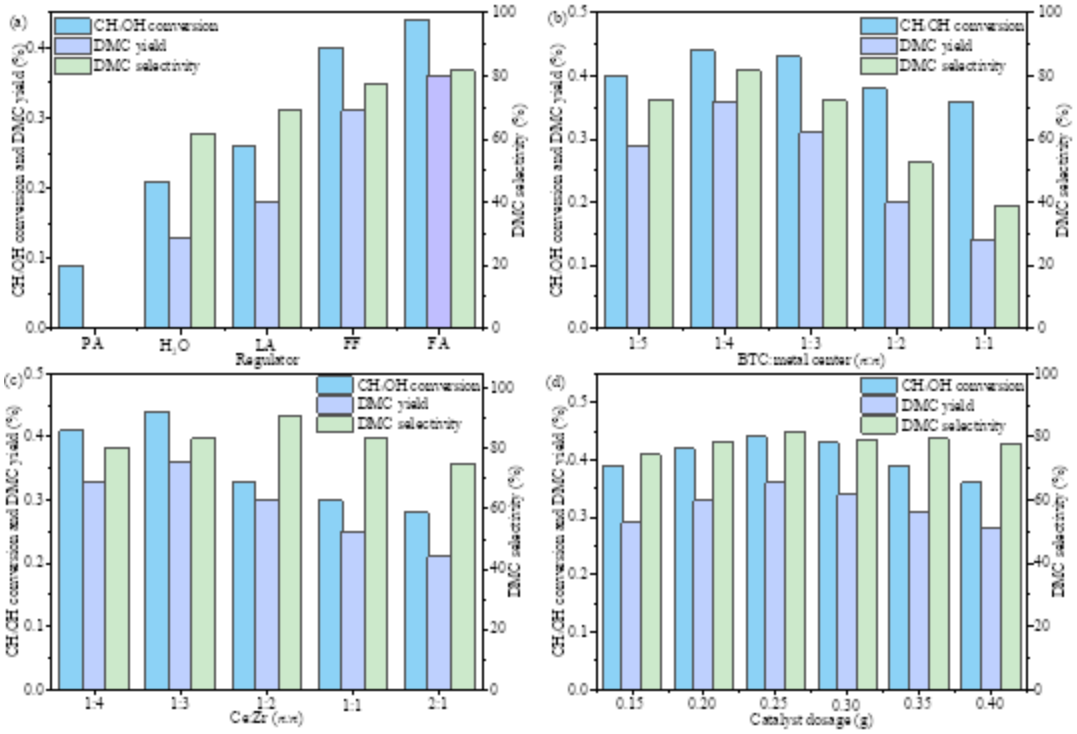


Figure 4

Effect of (a) regulator, (b) BTC/metal center molar ratio, (c) Ce/Zr molar ratio and (d) Ce/Zr-MOF-808 dosage on the conversion of CO_2 and CH_3OH to DMC. Reaction conditions: 8 mL CH_3OH, 11 MPa CO_2, reaction temperature 150 ℃, reaction time 12 h.

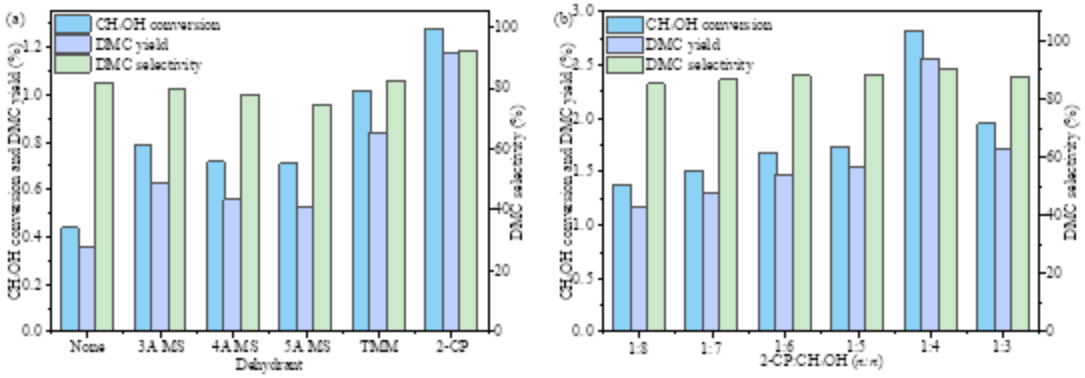


Figure 5

Effect of (a) dehydrant and its (b) dosage on the conversion of CO_2 and CH_3OH to DMC. Reaction conditions: FA as regulator, metal center : ligand=4:1, Ce:Zr=1:3, 0.25 g Ce/Zr-MOF-808 , 8 mL CH_3OH, 11 MPa CO_2, reaction temperature 150 ℃, reaction time 12 h.

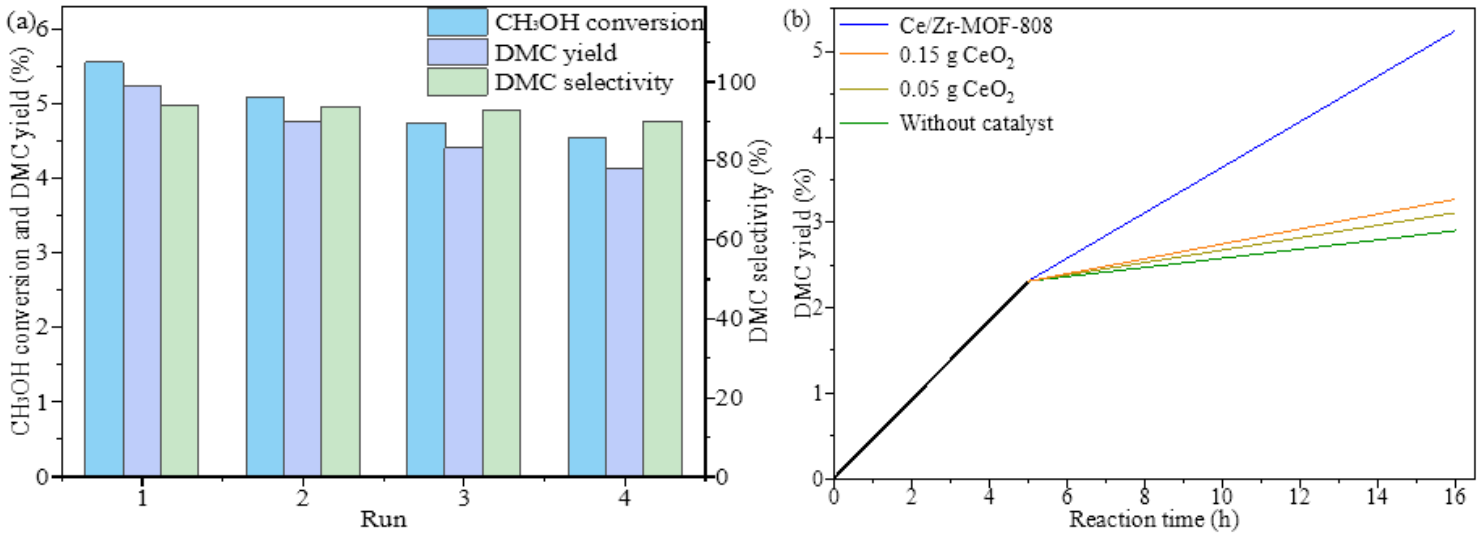


Figure 6

Recycling performance of Ce/Zr-MOF-808 (a) reusability and (b) leaching test. Reaction conditions: FA as regulator, metal center:ligand=4:1, Ce:Zr=1:3, 0.25 g Ce/Zr-MOF-808 , 8 mL CH_3OH, 2-CP:CH_3OH=1:4, 10 MPa CO_2, reaction temperature 140 ℃, reaction time 16 h.

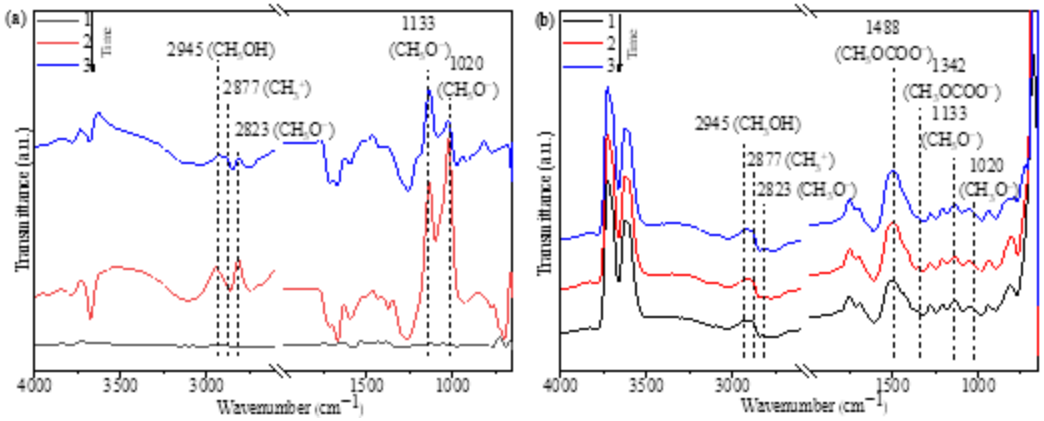


Figure 7

In situ FTIR of (a) adsorbed CH_3OH species and (b) preadsorbed with CH_3OH at 140 ℃ followed by passing CO_2 on Ce/Zr-MOF-808.

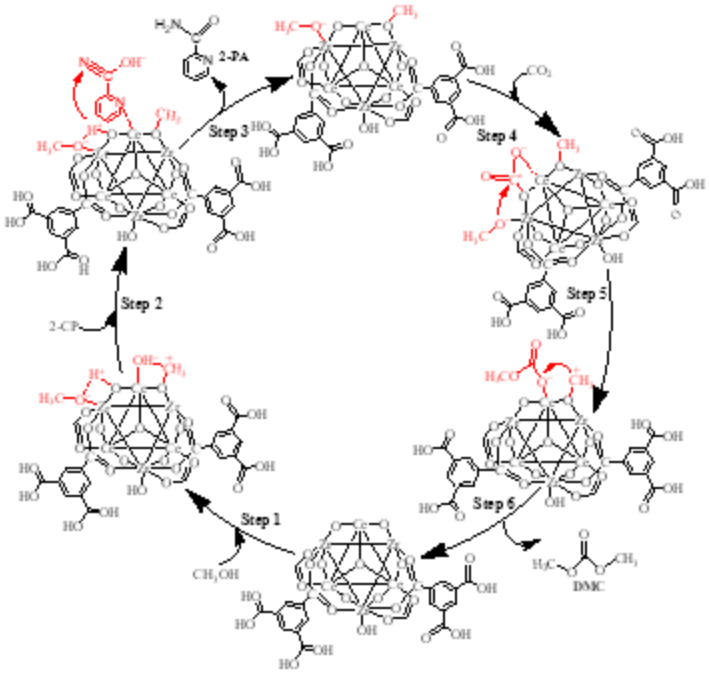


Figure 8

Plausible mechanism for the conversion of CO_2 and CH_3OH to DMC over Ce/Zr-MOF-808.

Supplementary Files

This is a list of supplementary files associated with this preprint. Click to download.

- Supplementarymaterial.docx